Progression of cell-to-cell variation within battery modules under different cooling structures

Ziyou Song [a,b], Niankai Yang [c,*], Xinfan Lin [d], Fanny Pinto Delgado [b], Heath Hofmann [b], Jing Sun [c]

[a] *Department of Mechanical Engineering, National University of Singapore, Singapore 117575, Singapore*
[b] *Department of Electrical Engineering and Computer Science, University of Michigan, Ann Arbor, MI 48109, USA*
[c] *Department of Naval Architecture and Marine Engineering, University of Michigan, Ann Arbor, MI 48109, USA*
[d] *Mechanical and Aerospace Engineering, University of California at Davis, Davis, CA 95616, USA*

HIGHLIGHTS

- An electro-thermal-aging model for battery module and coolant is established.
- Progression of cell-to-cell variation among parallel-connected cells is investigated.
- Influences of various cooling structures on cell-to-cell variation are analysed.
- A uniform cooling condition can significantly reduce cell-to-cell variation.

ARTICLE INFO

ABSTRACT

Cell-to-cell variation generally exists within battery packs, due to factors attributed to manufacturing and operating. Non-uniform temperature distribution, caused by the uneven cooling condition, contributes significantly to cell-to-cell variation over time, particularly to capacity variation, as temperature significantly influences the battery degradation rate. Especially for parallel-connected cells, the lack of individual current sensing and actuation makes it challenging to detect and control the capacity variation. In order to understand how cell-to-cell variation evolves, we investigate the effect of cooling structures on the progression of variation within parallel-connected battery cells using an electro-thermal-aging model for battery cells and a thermal model of the cooling system. The simulation result shows that the cell-to-cell variations increase initially because of uneven cooling conditions, but then the variation decreases over time, thanks to the self-balancing mechanism among parallel-connected cells. Moreover, when comparing the sequential and round cooling structures, it is found that the round cooling structure, which provides a more uniform cooling condition to all cells, has significant advantage in terms of suppressing the cell-to-cell variation, especially for large battery strings. The even cooling structure is preferred in practical applications; however, the trade-off between cooling system complexity and performance needs to be carefully considered.

1. Introduction

The Lithium-ion battery has been extensively utilized in electrified vehicles and renewable energy systems [1]. To meet power and energy requirements, individual cells need to be connected in parallel and series to constitute large battery packs. Ideally, the Battery Management System (BMS) needs to monitor all cells simultaneously, which is challenging in the presence of inevitable cell-to-cell variations caused by manufacturing processes and operating conditions [2]. For example, fresh cells even show apparent capacity variation after 10-month storage under the same environment [3]. Schuster et al. [4] experimentally characterized the capacity and impedance of 484 fresh and 1908 used lithium-ion battery cells, and it is found that cell-to-cell variation is significantly intensified after a 3-year operation in electric vehicles. Research has also shown that temperature has significant impact on battery aging [5], and non-uniform aging is the most prominent

contributor to cell-to-cell variation [6]. Series-connected battery cells use current and voltage sensors for every individual cell [7], and therefore BMS can effectively monitor and control the cell operation and balance the power among cells with non-uniform characteristics. However, it is challenging to monitor parallel-connected battery cells, since generally only one current and one voltage sensor is available [8]. The insufficient current sensing and actuation makes the health condition of individual cells hard to be observed and induces no controllability.

While uniform cooling condition for all cells is preferred in practice, it is almost infeasible to achieve due to the space and cost constraint [9]. Without uniform cooling, even though cell-to-cell variation is inevitable, the progression of variation can be impacted by different cooling structures, and warrant investigated. The non-uniform temperature distribution will cause the resistance variation and then result in current imbalance among various cells. As a result, individual cells will degrade at different rates, aggravating cell-to-cell variation, particularly capacity variation, which will impact battery performance, especially for large battery packs [10].

There have been studies on cell-to-cell variation within battery packs in the literature. For series-connected cells, Paul et al. [11] considered the variation in initial capacity and internal resistance, and they found that cells aged at different rates because of the current imbalance. Chiu et al. [12] emphasized the influence of temperature distribution and verified that a battery pack degrades faster with an increasing temperature variation. In terms of parallel-connected battery cells, Shi et al. [2] investigated the imbalance in current distribution among cells and showed that battery degradation will significantly decrease with reduced variation in cell temperature and current. Dubarry et al. [13] simulated battery packs with various configurations and chemistries, and then analyzed the intrinsic cell-to-cell variations induced by differences in initial states, capacities, and parameters. Offer et al. [14] experimentally examined how non-uniform inter-cell contact resistance induces current imbalance in a battery pack. Feng et al. [15] established a thermal-electrochemical model, and the simulation results show that 5 °C increase in temperature difference among the battery pack can lead to 1.5%–2% capacity loss of the battery pack, therefore temperature non-uniformity should be carefully considered in series-connected cells. Bruen and Marco [16] quantified the influence of uneven impedance on current imbalance and indicated that a 30% difference in impedance can cause a significant difference in cell current (~60%) and charge throughput (>6%). Assuming similar temperature among individual cells, an analytical investigation on how the cell-to-cell variations in terms of current, State of Charge (SoC), and aging rate, progress over time was performed [6]. Yang et al. [17] showed that temperature differences can directly result in imbalanced discharging and aging among parallel-connected cells. Liu et al. [18] found that heterogeneous overpotentials due to the interconnects (e.g. tabs and wiring) and uneven temperature distribution may significantly impair the performance of battery packs. Both [17 and 18] indicated that the cooling system plays an important role in such studies. To monitor cell inconsistency, Feng et al. proposed novel diagnostic algorithms for evaluating and estimating the cell-to-cell variation of parameters [19]. Tian et al. extracted multiple features to evaluate battery consistency and then proposed a novel algorithm to cluster battery packs [20].

However, the mechanisms associated with how the variation among parallel-connected cells progresses, are little understood, even though there are some initial reports. Chang et al. adopted a simple circuit model consisting of a resistance and a capacitance in series to study a battery string including 2 cells in series, and the simulation results show that the uniform cell resistance and capacity among cells can effectively reduce the inhomogeneities in SoC [21]. Baumann et al. examined the aged cells from a retired vehicle battery pack with a 2p96s configuration and found a self-balancing effect inside the parallel connection [22]. Rumpf et al. investigated the inhomogeneous current distribution in two parallel connected cells under constant current conditions, and the inhomogeneous current distribution induces variations in cell capacity,

cell impedance, and ambient temperature [23]. Note that there are some conflicting conclusions in the existing literature. For example, Fernández et al. [24] investigated a module of four battery cells in parallel and experimentally validated that an initial State of Health difference of 40% is reduced to 10% after 500 cycles, indicating that capacity variation diminishes over time. However, Gong et al. [25] concluded that the variation among cells will increase and cause an accelerated degradation. Even though a similar topic was focused in [6], the complete thermal model of battery string, especially the models under different cooling structures, was not covered, and the temperatures of all cells are assumed to be uniform. However, temperature is a key factor influencing cell degradation rate and inducing variations among cells. As a result, a quantitative study on cell-to-cell variation under practical cooling conditions is crucial and necessary.
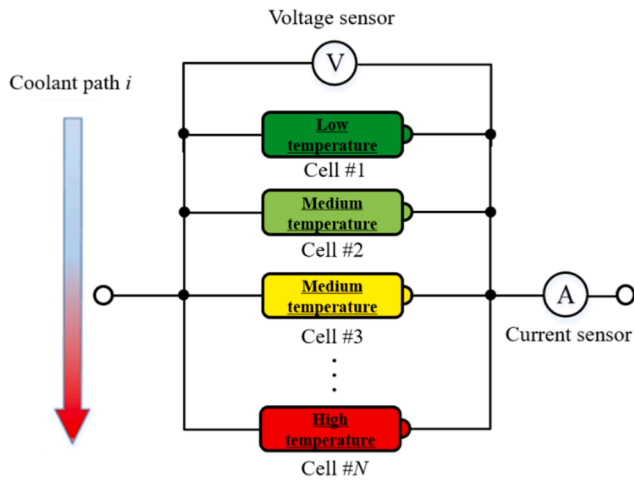
To fill the gap in the state of art, this paper investigates how capacity variation progresses among parallel-connected battery cells under different cooling structures. Two cooling structures, i.e., sequential cooling (a single coolant flow channel) and round cooling (two symmetric coolant flow channels), will be studied and compared. The temperature distribution among cells is analyzed based on the thermal model and used to determine the resistance imbalance, since the internal resistance is significantly influenced by temperature. In addition, current redistribution determined by the different resistance among cells is investigated based on the electric model. The temperature and current imbalances are used as the inputs of the battery degradation model to show how the capacity variation progresses. Simulation results reveal that cell-to-cell variation increases first due to the uneven cooling condition, and then decreases and settles after reaching the maximum value due to the self-balancing effect among parallel-connected battery cells [6]. In addition, capacity variation can be reduced by using a round cooling structure as compared to a sequential cooling structure, confirming that uniform cooling is favorable for keeping individual cells consistent.

The rest of the paper is organized as follows. The battery string model is presented in Section 2. In Section 3, simulation results and analysis are provided to show how different cooling structures impact the progression of cell-to-cell variations. Discussion of results is given in Section 4. In Section 5, conclusions are summarized.
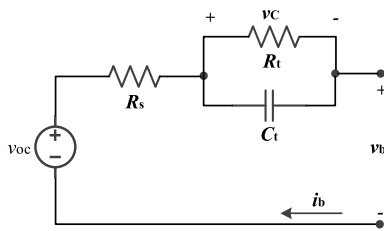
2. System modeling

The complete electro-thermal-aging model for parallel connected battery cells has not been found in the existing studies, but some individual models have been discussed. For example, Fill et al. proposed an electrical model for parallel-connected cells and strings, which incorporates the open circuit voltage (OCV) and ohmic resistance for each cell [26]. Even though this is a simplified electrical model, the experimental results show satisfactory accuracy. Then Fill et al. employed this model for the detection of a single cell contact loss within parallel-connected cells [27]. Similarly, Cai et al. also provided a simplified model for large-scale battery packs including both healthy and unhealthy cells based on the OCV-R model for individual cells [28]. Han et al. focused on the electrical model of series–parallel-connected battery strings and adopted the first-order equivalent circuit model for single cells, and this model is used for string-level State of Power estimation [29]. Considering the electrical model in [29] and a thermal model, Hosseinzadeh et al. investigated the current and temperature variations among cells under different battery configurations, and it shows that the Z shape module outperforms the ladder one [30]. Liu et al. simulated 6 battery cells connected in parallel based on a thermally coupled single particle model and the experimentally validated simulations show that cell-to-cell variation can be caused by the heterogeneous interconnect [18]. Furthermore, based on this model, Yang et al. presented an optimal charging strategy to minimize the lithium plating of a parallel battery module [31].

However, the above studies did not consider the cell aging model and

(a) Schematic of parallel battery string

(b) Equivalent circuit model for single cells

Fig. 1. Schematic of battery electric model.

the practical cooling structures, and therefore the progression of cell-to-cell variation in terms of capacity has not been investigated and is still unknown. To address this issue, an electro-thermal-aging model for parallel-connected battery cells under different cooling structures is introduced in this section.

2.1. Battery string modeling

Consider an N-cell parallel battery string under non-uniform cooling condition, as shown in Fig. 1 (a). The terminal voltage of all cells is

The dynamics of a single cell in the state space form are described as [33]:

$$\begin{bmatrix} \dot{v}_{\text{OC},j} \\ \dot{v}_{\text{C},j} \end{bmatrix} = \begin{bmatrix} 0 & 0 \\ 0 & -\dfrac{1}{\tau_j} \end{bmatrix} \cdot \begin{bmatrix} v_{\text{OC},j} \\ v_{\text{C},j} \end{bmatrix} + \begin{bmatrix} \alpha_j \\ \dfrac{R_{\text{t},j}}{\tau_j} \end{bmatrix} \cdot i_{\text{b},j} \tag{1}$$

$$v_{\text{b}} = \begin{bmatrix} 1 & -1 \end{bmatrix} \cdot \begin{bmatrix} v_{\text{OC},j} \\ v_{\text{C},j} \end{bmatrix} - R_{\text{s},j} i_{\text{b},j} \tag{2}$$

where v_{OC} denotes cell OCV, v_{b} denotes cell terminal voltage, i_{b} denotes cell current (negative for charging), R_{s} denotes cell ohmic resistance, v_{C}, R_{t}, τ denote voltage, diffusion resistance, and time constant of RC circuit, and j represents the cell index and will be used in the following formulations. In addition, α denotes the rate of OCV change driven by current and is given by

$$\alpha_j = -\frac{a\eta}{Q_{\text{b},j}} \tag{3}$$

where Q_{b} is the cell capacity, a is the slope of the OCV- SoC curve, and η is the coulombic efficiency of charge/discharge. Note that most OCV-SoC functions are nonlinear over the whole SoC region [34], but can be approximated as a linear function within the central SOC range (i. e., the normal operating region for batteries) for most chemistries [35,36].

In consequence, a linearized OCV-SoC function is adopted in Eq. (1). By extending the battery string model of two cells in [6], we can derive the general dynamic model for the N-cell battery string as

$$\dot{x}_s = A \cdot x_s + B \cdot \begin{bmatrix} i_{\text{b},1} & i_{\text{b},2} & \cdots & i_{\text{b},N} \end{bmatrix}^T \tag{4a}$$

$$v_{\text{b}} = C \cdot x_s + D \cdot \begin{bmatrix} i_{\text{b},1} & i_{\text{b},2} & \cdots & i_{\text{b},N} \end{bmatrix}^T \tag{4b}$$

$$A = \begin{bmatrix} 0 & 0 & 0 & 0 & \cdots & 0 & 0 \\ 0 & -\dfrac{1}{\tau_1} & 0 & 0 & \cdots & 0 & 0 \\ 0 & 0 & 0 & 0 & \cdots & 0 & 0 \\ 0 & 0 & 0 & -\dfrac{1}{\tau_2} & \cdots & 0 & 0 \\ & & & & \ddots & & \\ 0 & 0 & 0 & 0 & \cdots & 0 & 0 \\ 0 & 0 & 0 & 0 & \cdots & 0 & -\dfrac{1}{\tau_N} \end{bmatrix}, B = \begin{bmatrix} \alpha_1 & 0 & \cdots & 0 & 0 \\ \dfrac{R_{\text{t},1}}{\tau_1} & 0 & \cdots & 0 & 0 \\ 0 & \alpha_2 & \cdots & 0 & 0 \\ 0 & \dfrac{R_{\text{t},2}}{\tau_2} & \cdots & 0 & 0 \\ & & \ddots & & \\ 0 & 0 & \cdots & 0 & \alpha_N \\ 0 & 0 & \cdots & 0 & \dfrac{R_{\text{t},N}}{\tau_N} \end{bmatrix},$$

$$C = \begin{bmatrix} 1 & -1 & 0 & \cdots & 0 \end{bmatrix}, D = \begin{bmatrix} -R_{\text{s},1} & 0 & \cdots & 0 \end{bmatrix}, x_s = \begin{bmatrix} v_{\text{OC},1} & v_{\text{C},1} & v_{\text{OC},2} & v_{\text{C},2} & \cdots & v_{\text{OC},N} & v_{\text{C},N} \end{bmatrix}^T$$

measured by a voltage sensor, and the total current is measured by a current sensor. The resistance and capacity imbalance among cells caused by the temperature distribution will result in non-uniform current distribution, which will be investigated based on the electric model of the battery string. The first-order equivalent circuit model is adopted to capture the electric dynamics of single cells with adequate fidelity and complexity [32], as shown in Fig. 1 (b). The cell-to-cell variation is characterized by the difference among cells in capacity and resistance. Note that in the cooling systems focused in this study, coolant is contained in the channel (e.g., pipes) and not free on the cell surface. All parameters of thermal models adopted in the simulation are assumed based on the heat transfer between the coolant channel and cell surface, such as the convective heat transfer coefficient h.

where A, B, C, D are the matrices of the state space function governing the electrical model of battery strings, and x_s is the state vector, including OCV and RC voltage of different cells in the string. The total current equals to the sum of individual current (see Eq. (1)) and the voltage of each cell are the same (see Eq. (2)). Hence based on the Kirchhoff's laws, we can obtain the relationship between the individual cell currents and the total current i_{bs}, as given below.

$$R \cdot \begin{bmatrix} i_{\text{b},1} & i_{\text{b},2} & \cdots & i_{\text{b},N} \end{bmatrix}^T = E \cdot x_s + F \cdot i_{\text{bs}} \tag{5}$$

where

$$\mathbf{R} = \begin{bmatrix} 1 & 1 & 1 & \cdots & 1 & 1 \\ -R_{s,1} & R_{s,2} & 0 & \cdots & 0 & 0 \\ 0 & -R_{s,2} & R_{s,3} & \cdots & 0 & 0 \\ & & & \ddots & & \\ 0 & 0 & 0 & & -R_{s,N-1} & R_{s,N} \end{bmatrix}, \; \mathbf{E} = \begin{bmatrix} 0 & 0 & 0 & 0 & 0 & \cdots & 0 & 0 & 0 & 0 \\ -1 & 1 & 1 & -1 & 0 & \cdots & 0 & 0 & 0 & 0 \\ 0 & -1 & 1 & 1 & -1 & \cdots & 0 & 0 & 0 & 0 \\ & & & & & \ddots & & & & \\ 0 & 0 & 0 & 0 & \cdots & -1 & 1 & 1 & -1 \end{bmatrix}, \; \mathbf{F} = \begin{bmatrix} 1 \\ \vdots \\ 0 \end{bmatrix}$$

$\mathbf{R}$ is the matrix containing ohmic resistance of all cells in the string, and $\mathbf{E}$ and $\mathbf{F}$ are the matrices indicating the relationship between total current and cell current and how current is distributed. Therefore, the current distribution can be derived based on Eq. (5) as follows

$$\begin{bmatrix} i_{b,1} & i_{b,2} & \cdots & i_{b,N} \end{bmatrix}^T = \mathbf{R}^{-1}\mathbf{E}{\cdot}\mathbf{x}_s + \mathbf{R}^{-1}\mathbf{F}{\cdot}i_{bs} \tag{6}$$

Based on Eqs. (3) and (6), the electric model of the battery string with cells connected in parallel can be given as

$$\dot{\mathbf{x}}_s = (\mathbf{A} + \mathbf{B}\mathbf{R}^{-1}\mathbf{E}){\cdot}\mathbf{x}_s + \mathbf{B}\mathbf{R}^{-1}\mathbf{F}{\cdot}i_{bs} \tag{7}$$

$$v_b = (\mathbf{C} + \mathbf{D}\mathbf{R}^{-1}\mathbf{E}){\cdot}\mathbf{x}_s + \mathbf{D}\mathbf{R}^{-1}\mathbf{F}{\cdot}i_{bs} \tag{8}$$

The thermal model of battery cells is also incorporated as the temperature information is critical in this study. A control-oriented thermal model, which captures the surface and core temperatures of a battery cell as two states, is adopted as it provides adequate fidelity with moderate complexity [37] when compared with the single-state model [38] and the partial differential equation-based electrochemical-thermal model [39]. The adopted thermal model has been experimentally validated for cylindrical battery cells assuming peripheral and longitudinal homogeneities [36]. Note that, for the pouch and prismatic cells, a more complicated and accurate model is required to characterize the dynamics of the core temperature [40], which will be significantly different from the surface temperature under aggressive current profiles [37]. The governing equations of the adopted thermal model are

$$\begin{cases} C_c\dot{T}_{bc,j} = i_{b,j}^2(R_{s,j} + R_{t,j}) + \dfrac{T_{bs,j} - T_{bc,j}}{R_{in}}, \\ C_s\dot{T}_{bs,j} = h(T_{f,j} - T_{bs,j}) - \dfrac{T_{bs,j} - T_{bc,j}}{R_{in}}, \end{cases} \tag{9}$$

where T_{bc} is the temperature at the cell core, T_{bs} is the temperature at the cell surface, $T_{f,j}$ is the coolant temperature at the jth cell, R_{in} is the lumped thermal resistance of conduction and contact between the cell core and surface, C_c is the heat capacity of cell core, C_s is the heat capacity of cell surface, and h is the convective heat transfer coefficient between the cell surface and the coolant channel. We assume that there is no variation among cells in terms of thermal parameters including R_{in}, C_c, C_s, and h. Note that only joule heat is considered in heat generation, and both Ohmic resistance R_s and polarization resistance R_t will contribute to heat generation as a constant-current profile will be used in the simulation [34].

The degradation process of the lithium-ion battery cell over its lifetime includes an approximately linear phase and a nonlinear phase [41]. The linear phase indicates the gradual aging because of the growth of solid electrolyte interphase layer, while the nonlinear phase represents the fast-aging stage near the battery end of life [42] caused by severe lithium plating [41]. In electric vehicles, the battery should be changed when its capacity decreases to 80% of the nominal value (i.e., generally in the linear degradation phase). As a result, only the linear degradation phase is considered in this study. Wang et al. considered several key factors (i.e., depth of charge, temperature, and discharge rate) and proposed a semi-empirical degradation model for Lithium-ion batteries [43].

$$Q_{loss} = \frac{Q_{non} - Q_b}{Q_{non}} = Ae^{-\left(\frac{E_a + B \cdot C\_Rate}{RT_{bc}}\right)}(A_h)^z, \tag{10}$$

where Q_{loss} is the capacity loss which is normalized from 0 (i.e., minimum loss) to 1 (i.e., maximum loss), Q_{non} is the cell nominal capacity, Q_b is the cell remaining capacity at current cycle, E_a is the activation energy, A is the pre-exponential factor, R is the gas constant, A_h is the amp-hour-throughput, z is the exponential factor, C_Rate is the discharge (or charge) rate, and B is the compensation factor. However, the above degradation model can only be implemented over standard testing cycles (i.e., fully charging/discharging profiles with the fixed current). By discretizing the model in Eq. (10), a dynamic degradation model has been proposed and experimentally validated in [44], based on the cumulative damage theory [45]. The dynamic degradation model can be expressed as

$$Q_{loss}(t + \Delta t) - Q_{loss}(t) = \Delta A_h z A^{\frac{1}{z}} e^{-\left(\frac{E_a + B \cdot C\_Rate}{zRT_{bc}}\right)} Q_{loss}(t)^{\frac{z-1}{z}}, \tag{11}$$

where

$$\Delta A_h = \frac{1}{3600}\int_t^{t+\Delta t}|i_b|\mathrm{d}t$$

t is the time instant, and Δt is the sampling period. See [44] for the detailed information on the discrete model (i.e., Eq. (11)) and experimental verification.

2.2. Cooling system modeling

The thermal dynamics of coolant and the interaction between battery cells and the coolant channel are modeled in this section. While uniform cooling is desirable for reduced cell-to-cell variation, it is difficult to achieve in real-world applications owing to space and cost constraints. In this study, we consider two practical cooling structures (i.e., sequential and round cooling structures), as shown in Fig. 2, for a battery string with N cells connected in parallel, assuming no initial variation among cells and absolute thermal insulation between adjacent cells (i.e., no heat transfer among cells). The radiant heat transfer among cells is neglected to simplify the thermal model. Specifically, given the low emissivity of the silver surface of cells, the small temperature difference between the adjacent cells, and the small area of surface exposed to radiant heat transfer, the radiant heat transfer is negligible, especially when the cells are often not in contact with each other in a commercial battery pack (e.g., Tesla Model S).

First, as shown in Fig. 2, a thermal model for battery strings is constructed based on the aforementioned thermal model of single cells (see Eq. (10)). The sequential cooling structure, as shown in Fig. 2 (a), only includes one coolant channel, and all cells are placed along the channel. So the coolant absorbs the heat dissipated from the cell surface via convection and is therefore heated from inlet to outlet. The cells at the inlet and outlet of coolant have the best and worst cooling conditions, respectively, given the temperature gradient of coolant. The coolant temperature at the jth cell, denoted as $T_{f,j}$, is dependent on the heat balance of the coolant flow at the $(j{\text -}1)^{th}$ cell. The temperature increase of coolant (i.e., $T_{f,j}–T_{f,j-1}$) can be obtained by dividing the dissipated heat from the $(j{\text -}1)^{th}$ cell with the heat capacity of the coolant, i.e., C_f. The

coolant temperature at the inlet (i.e., the 1st cell) $T_{f,in}$ can be regulated by the thermal management system. Detailed modeling of the coolant thermal dynamics has been discussed in [47] and the discretized formulation takes the form

$$T_{f,j} = \begin{cases} T_{f,in}, & j = 1, \\ T_{f,j-1} - \dfrac{h\Delta t}{C_f}\left(T_{f,j-1} - T_{bs,j-1}\right), & j = 2, 3, \cdots N, \end{cases} \tag{12}$$

where C_p is the specific heat capacity of the coolant (J/kg·K), C_f (i.e., equals to $C_p V_{cool} \Delta t$) represents the heat capacity of the flowing coolant (J/K), and V_{cool} is the coolant flow rate (kg/s), which is a decision variable of the thermal management system. The heat capacity of coolant should be adjusted according to the total number of cells and the battery operating condition; therefore, it should be adjusted proportionally according to the cell number, meaning that the larger battery pack requires a better cooling capability. Assuming the thermal parameters of various cells (i.e., C_c, C_s, and R_{in}) are the same and constant, the coolant temperature at different locations can be obtained based on Eq. (12).

$$\begin{cases} T_{f,j} = \left(1 - \dfrac{h}{C_{f0}}\right)^2 T_{f,j-2} + \dfrac{h}{C_{f0}}\left(1 - \dfrac{h}{C_{f0}}\right)T_{bs,j-2} + \dfrac{h}{C_{f0}}T_{bs,j-1}, \\ T_{f,j-2} = \left(1 - \dfrac{h}{C_{f0}}\right)T_{f,j-3} + \dfrac{h}{C_{f0}}T_{bs,j-3}, \end{cases} \tag{13}$$

where $C_{f0} = C_p(NV_{cool})$ (W/K). As mentioned above, C_{f0} is the heat capacity of coolant and proportional to the cell number to ensure the thermal model is reasonably set.

Based on Eqs. (12) and (13), the following equation can be derived recursively for computing the distributed coolant temperature

$$T_{f,j} = \left(1 - \dfrac{h}{C_{f0}}\right)^{j-1} T_{f,in} + \dfrac{h}{C_{f0}}\left(1 - \dfrac{h}{C_{f0}}\right)^{j-2} T_{bs,1} + \dfrac{h}{C_{f0}}\left(1 - \dfrac{h}{C_{f0}}\right)^{j-3} T_{bs,2}$$
$$+ \cdots + \dfrac{h}{C_{f0}}T_{bs,j-1} \tag{14}$$

As a result, the thermal model under the sequential cooling structure can be represented in state space as

$$\dot{x}_T = A_{TS} \cdot x_T + B_{TS} \cdot u_T \tag{15}$$

where

$$A_{TS} = \begin{bmatrix} \dfrac{-1}{R_{in}C_c} & \dfrac{1}{R_{in}C_c} & 0 & 0 & \cdots & 0 & 0 & 0 \\ \dfrac{1}{R_{in}C_s} & \dfrac{-1}{C_s}\left(h + \dfrac{1}{R_{in}}\right) & 0 & 0 & \cdots & 0 & 0 & 0 \\ 0 & 0 & \dfrac{-1}{R_{in}C_c} & \dfrac{1}{R_{in}C_c} & \cdots & 0 & 0 & 0 \\ 0 & \dfrac{h^2}{C_s C_{f0}} & \dfrac{1}{R_{in}C_s} & \dfrac{-1}{C_s}\left(h + \dfrac{1}{R_{in}}\right) & \cdots & 0 & 0 & 0 \\ & & & & \ddots & & & \\ 0 & 0 & 0 & 0 & \cdots & 0 & \dfrac{-1}{R_{in}C_c} & \dfrac{1}{R_{in}C_c} \\ 0 & \dfrac{h^2}{C_s C_{f0}}\left(1 - \dfrac{h}{C_{f0}}\right)^{N-1} & 0 & \dfrac{h^2}{C_s C_{f0}}\left(1 - \dfrac{h}{C_{f0}}\right)^{N-2} & \cdots & \dfrac{h^2}{C_s C_{f0}} & \dfrac{1}{R_{in}C_s} & \dfrac{-1}{C_s}\left(h + \dfrac{1}{R_{in}}\right) \end{bmatrix}$$

$$B_{TS} = \begin{bmatrix} \dfrac{(R_{s,1} + R_{t,1})}{C_c} & 0 & 0 & \cdots & 0 & 0 & 0 & 0 & \cdots & 0 \\ 0 & 0 & 0 & \cdots & 0 & \dfrac{h}{C_s} & 0 & 0 & \cdots & 0 \\ 0 & \dfrac{(R_{s,2} + R_{t,2})}{C_c} & 0 & \cdots & 0 & 0 & 0 & 0 & \cdots & 0 \\ 0 & 0 & 0 & \cdots & 0 & 0 & \dfrac{h}{C_s}\left(1 - \dfrac{h}{C_{f0}}\right) & 0 & \cdots & 0 \\ & & & \ddots & & & & & \ddots & \\ 0 & 0 & 0 & \cdots & \dfrac{(R_{s,N} + R_{t,N})}{C_c} & 0 & 0 & 0 & \cdots & 0 \\ 0 & 0 & 0 & \cdots & 0 & 0 & 0 & 0 & \cdots & \dfrac{h}{C_s}\left(1 - \dfrac{h}{C_{f0}}\right)^{N-1} \end{bmatrix}$$

$$x_T = \begin{bmatrix} T_{bc,1} & T_{bs,1} & T_{bc,2} & T_{bs,2} & \cdots & T_{bc,N} & T_{bs,N} \end{bmatrix}^T, \quad u_T = \begin{bmatrix} i_{b,1}^2 & i_{b,2}^2 & \cdots & i_{b,N}^2 & T_{f,in} & T_{f,in} & \cdots & T_{f,in} \end{bmatrix}^T.$$

$\mathbf{A_{TS}}$ and $\mathbf{B_{TS}}$ denote the matrices of the state space function related to the battery string under sequential cooling structure, $\mathbf{x_T}$ is the state vector including the core and surface temperatures of all cells, and $\mathbf{u_T}$ is the input vector containing individual cell current and coolant temperature at inlet, which can be controlled to regulate the cell temperature.

The round cooling structure, as shown in Fig. 2 (b), provides two symmetric coolant channels that lead to a more uniform cooling condition compared to the sequential cooling structure. For fair comparison, we assume that two cooling structures have the same cooling capacity. Namely, the heat capacity of each coolant channel of the round cooling structure is reduced to half of the one of the sequential cooling structure (i.e., $0.5C_f$), resulting in the total heat capacity of C_f. Following a similar procedure, the thermal model under the round cooling structure can be derived in state space as

$$\dot{\mathbf{x}}_T = \mathbf{A}_{TR}\cdot\mathbf{x}_T + \mathbf{B}_{TR}\cdot\mathbf{u}_T \tag{16}$$

where

2.3. Integrated model

In this study, the time constant τ of battery cells in the electrical sub-model is assumed to be uniform among cells and invariant over time, while the electrical resistance will decrease with increasing temperature according to

$$\begin{aligned} R_{s,i} &= R_{s,0} + \kappa\big(T_{bc,i} - T_{bc,0}\big)R_{s,0}, \\ R_{t,i} &= R_{t,0} + \kappa\big(T_{bc,i} - T_{bc,0}\big)R_{t,0}, \end{aligned} \tag{17}$$

where κ is a constant coefficient, $T_{bc,0}$ is the nominal temperature at cell core (i.e., 15 °C), and $R_{s,0}$ and $R_{t,0}$ represent the cell ohmic and diffusion resistance at nominal temperature and initial capacity, respectively. In addition, the cell resistance will also increase with aging as

$$\begin{aligned} R_{s,j} &= \varepsilon\left(\frac{Q_{non}}{Q_{b,j}}\right)^{\lambda} R_{s,0}, \\ R_{t,j} &= \varepsilon\left(\frac{Q_{non}}{Q_{b,j}}\right)^{\lambda} R_{t,0}, \end{aligned} \tag{18}$$

$$\mathbf{A}_{TR} = \begin{bmatrix} \frac{-1}{R_{in}C_c} & \frac{1}{R_{in}C_c} & 0 & 0 & \cdots & 0 & 0 & 0 \\ \frac{1}{R_{in}C_s} & \frac{-1}{C_s}\left(h+\frac{1}{R_{in}}\right) & 0 & 0 & \cdots & \frac{h^2}{0.5C_sC_{f0}}\left(1-\frac{h}{0.5C_{f0}}\right)^{N-3} & 0 & \frac{h^2}{0.5C_sC_{f0}}\left(1-\frac{h}{0.5C_{f0}}\right)^{N-2} \\ 0 & 0 & \frac{-1}{R_{in}C_c} & \frac{1}{R_{in}C_c} & \cdots & 0 & 0 & 0 \\ 0 & \frac{h^2}{0.5C_sC_{f0}} & \frac{1}{R_{in}C_s} & \frac{-1}{C_s}\left(h+\frac{1}{R_{in}}\right) & \cdots & \frac{h^2}{0.5C_sC_{f0}}\left(1-\frac{h}{0.5C_{f0}}\right)^{N-4} & 0 & \frac{h^2}{0.5C_sC_{f0}}\left(1-\frac{h}{0.5C_{f0}}\right)^{N-3} \\ & & & & & & \ddots & \\ 0 & 0 & 0 & 0 & \cdots & 0 & \frac{-1}{R_{in}C_c} & \frac{1}{R_{in}C_c} \\ 0 & \frac{h^2}{0.5C_sC_{f0}}\left(1-\frac{h}{0.5C_{f0}}\right)^{N-2} & 0 & \frac{h^2}{0.5C_sC_{f0}}\left(1-\frac{h}{0.5C_{f0}}\right)^{N-3} & \cdots & \frac{h^2}{0.5C_sC_{f0}} & \frac{1}{R_{in}C_s} & \frac{-1}{C_s}\left(h+\frac{1}{R_{in}}\right) \end{bmatrix}$$

$$\mathbf{B}_{TR} = \begin{bmatrix} \frac{(R_{s,1}+R_{t,1})}{C_c} & 0 & 0 & \cdots & 0 & 0 & 0 & 0 & \cdots & 0 \\ 0 & 0 & 0 & \cdots & 0 & \frac{h}{C_s}+\frac{h}{C_s}\left(1-\frac{h}{0.5C_{f0}}\right)^{N-1} & 0 & 0 & \cdots & 0 \\ 0 & \frac{(R_{s,2}+R_{t,2})}{C_c} & 0 & \cdots & 0 & 0 & 0 & 0 & \cdots & 0 \\ 0 & 0 & 0 & \cdots & 0 & 0 & \frac{h}{C_s}\left(1-\frac{h}{0.5C_{f0}}\right)+\frac{h}{C_s}\left(1-\frac{h}{0.5C_{f0}}\right)^{N-2} & 0 & \cdots & 0 \\ \ddots & & & & & & & \ddots & & \\ 0 & 0 & 0 & \cdots & \frac{(R_{s,N}+R_{t,N})}{C_c} & 0 & 0 & 0 & \cdots & 0 \\ 0 & 0 & 0 & \cdots & 0 & 0 & 0 & 0 & \cdots & \frac{h}{C_s}\left(1-\frac{h}{0.5C_{f0}}\right)^{N-1}+\frac{h}{C_s} \end{bmatrix}$$

$\mathbf{A_{TR}}$ and $\mathbf{B_{TR}}$ denote the matrices of the state space function related to the battery string under round cooling structure. Note that the state and input vectors are same to the ones related to sequential cooling structure (see Eq. (15)).

where ε and λ are both pre-defined and constant coefficients ($\alpha > 1$, $\lambda \geq 1$).

The battery model proposed above can be generalized to different chemistries. Especially, the degradation model can achieve satisfactory accuracy for various battery chemistries with a careful calibration based on the cycling data [49]. Note that the adopted electrical model, thermal model, and aging model are organically coupled together, and this is not
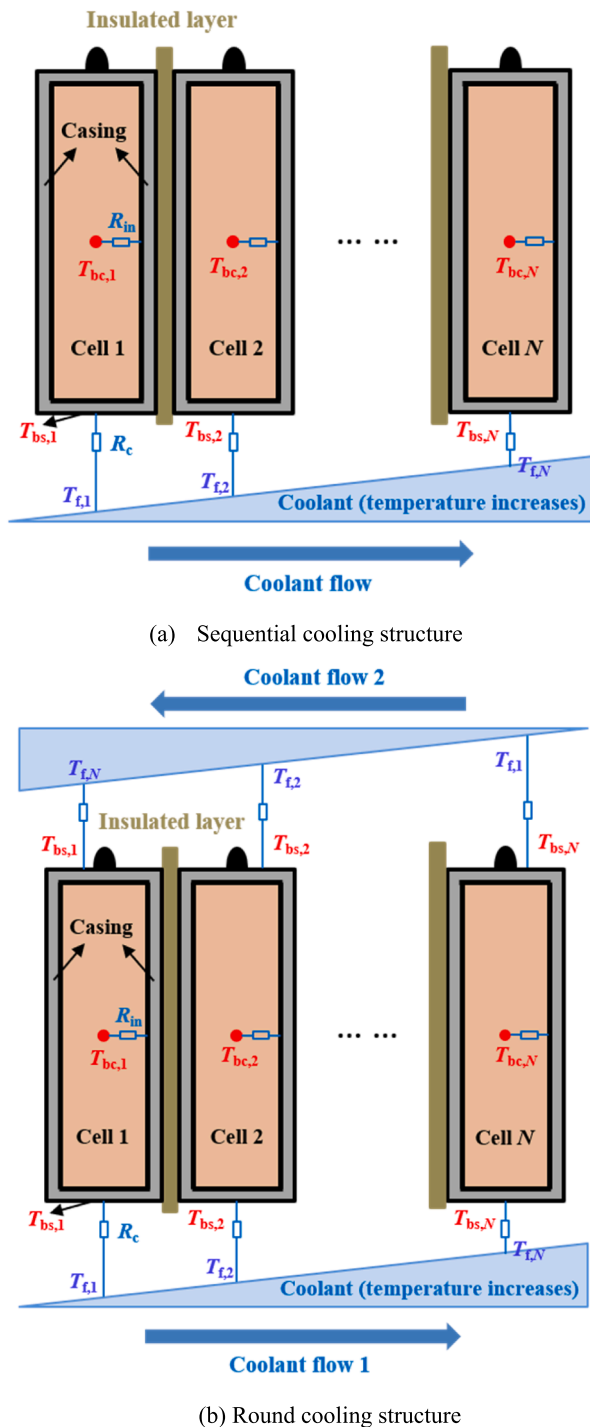
(a) Sequential cooling structure

(b) Round cooling structure

Fig. 2. Battery strings under different cooling structures.

a simple combination. The electrical, thermal, and aging characteristics significantly influence each other, and the evolution of the entire system is complex. For example, both degradation level and temperature will impact the battery internal resistance, which will determine the current distribution among cells (i.e., electrical behaviors). In turn, the cell current will remarkably affect its temperature and degradation rate. Therefore, the coupling relationship between different models is complicated and cannot be obtained without a throughout simulation. In addition, even though those individual models, including electrical model, thermal model, and aging model, have been well verified in the existing studies, we point out that it is worthwhile to experimentally

validate the entire model, given the complicated coupling relationship between individual models. However, it is time-consuming to establish the battery strings with various cooling systems and conduct the aging test, thus we will include experimental study in the future.

3. Simulation results

The continuous battery models are established in Matlab using the state-space model toolbox (i.e., ss function), then we use the lsim function to discretize the system and simulate the system responses, based on the initial system states, system inputs, and the desired sampling time. Based on the above model, simulation is conducted to analyze how cell-to-cell variation progresses under sequential and round cooling structures. It is assumed that no initial variation exists among cells. To visualize the obvious battery degradation, simulations are performed over 5000 h for the expedited aging study. To reduce the computational time, the sampling time is chosen as 30 s and the battery string is repeatedly charged and discharged at 4C rate starting from 60% SoC. In practical applications, battery is generally not cycled at such a high current because it will significantly speed up the degradation. For example, the maximum current is usually below 2C in electric vehicle applications [48]. In this study, the current is elevated to 4C to expedite the degradation process. Note that current magnitude will not affect the conclusions in the following analysis, as the individual cell current and degradation rate will just positively correlate to the total current, and therefore a similar trend for cell-to-cell variation can be obtained. The capacity variation, which is denoted as Q_{sv}, is quantified as:
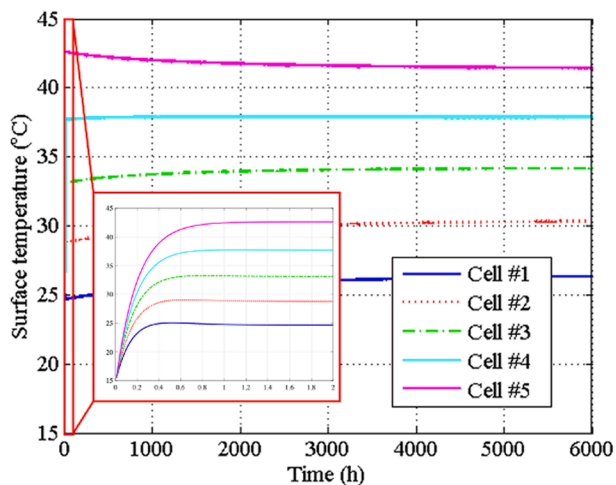
$$Q_{sv} = \frac{1}{N-1} \sum_{i=1}^{N} \left[Q_{bi} - \frac{1}{N} \sum_{i=1}^{N} (Q_{bi}) \right]^2 \tag{19}$$

The electric model (see Eqs. (7) and (8)), the degradation model (see Eq. (11)), and the thermal model (see Eqs. (15) and (16)) are adopted in simulation. The specifications of the simulation setup are listed in Table 1.
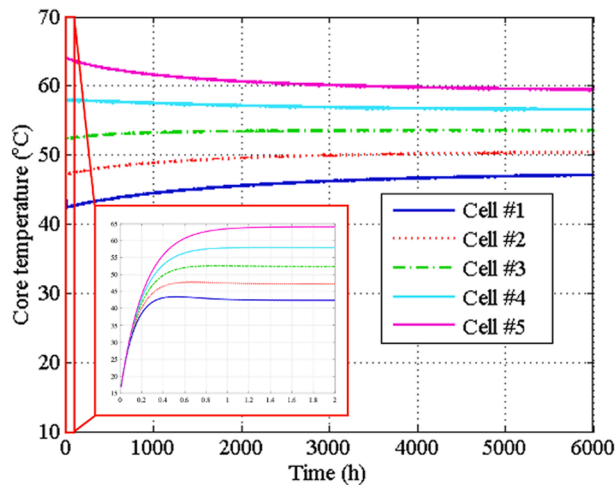
We first investigate a five-cell battery string under different cooling structures. For the sequential cooling structure, as shown in Fig. 3 (a) and 3 (b), the surface and core temperatures of different cells follow the same pattern during testing. Specifically, cell temperatures start from 15 °C and then diverge due to the uneven cooling condition. For all individual cells, core temperatures are higher than surface temperatures, and the temperature gradient inside the cell is significant under

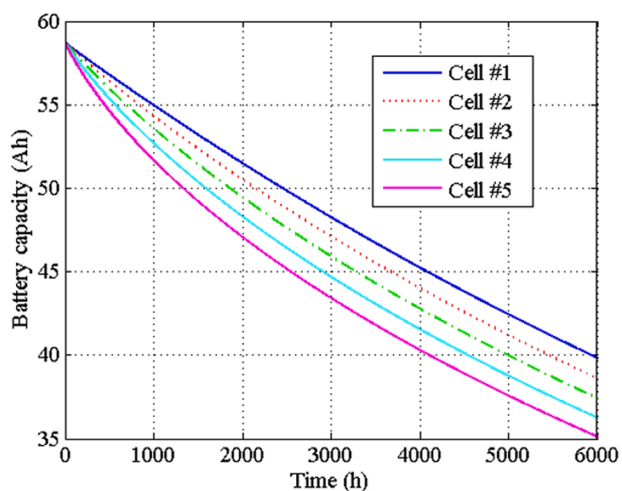**Table 1**
Simulation specifications.

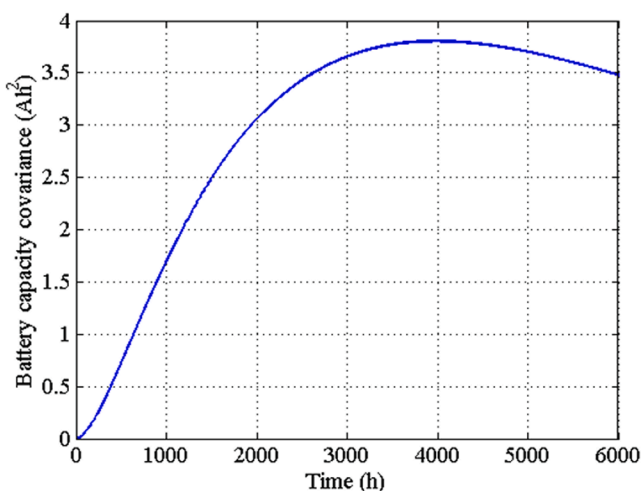| Parameter	Value
Cell initial capacity (Ah)	58.7
Time constant of RC pair τ (s)	~4
Ohmic resistance of cell R_s (mΩ)	~1
Diffusion resistance of cell R_t (mΩ)	~1
Charge/discharge efficiency η	0.99
Slope of OCV-SoC curve a (mV/%)	~1.5
Pre-exponential factor in degradation model A	0.0032
Compensation factor in degradation model B	1516
Activation energy in degradation model E_a (J)	15,162
Exponential factor in degradation model z	0.824
Gas constant R (J/(mol·K))	8.314
Core heat capacity of cell C_c (J/K)	2100
Surface heat capacity of cell C_s (J/K)	200
Lumped thermal resistance within cell R_{in} (K/W)	0.183
Coefficient of convective heat transfer between coolant channel and cell surface h (W/K)	10
Initial temperature of battery and coolant (°C)	15
Coefficient ε in Eq. (18)	1.2
Coefficient λ in Eq. (18)	2
Coefficient κ in Eq. (17)	0.0067
Specific heat capacity of coolant C_p (J/kg·K)	3140
Sampling time in simulation Δt (s)	30
Numbers of cells in battery strings in the simulation	5 and 20

(a) Surface temperature

(b) Core temperature

(c) Cell capacities

(d) Capacity variation

Fig. 3. Temperature and Capacity Evolution of battery string (5 cells) under sequential cooling structure.
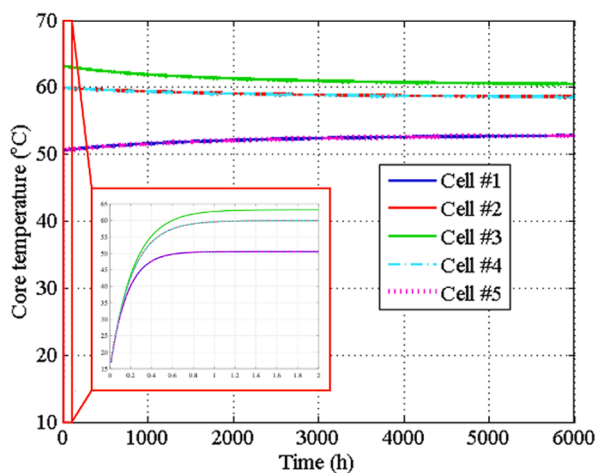
the aggressive current profile. As the cell resistance decreases with an increasing temperature in the normal temperature range, Cell #5 at the outlet has the lowest resistance and highest current among all cells. Given that the battery degradation rate positively correlates to the core temperature and current amplitude (see Eq. (11)), Cell #1 has the lowest degradation, and Cell #5 suffers the largest degradation over time, as shown in Fig. 3 (c).

The results verify that the non-uniform cooling condition will generate cell-to-cell variation among the parallel-connected cells. Note that the above observation regarding distributions of degradation and resistance is valid at normal temperatures (e.g., 0 °C to 40 °C) and may be opposite at extremely low temperatures as higher core temperature may reduce degradation when the environmental temperature is low. The capacity variation among cells, as shown in Fig. 3 (d), will increase first and slightly decrease after reaching the maximum value (i.e., 4000 h). This shows that the capacity variation caused by uneven cooling is suppressed by a self-balancing effect existing within cells connected in parallel [6].
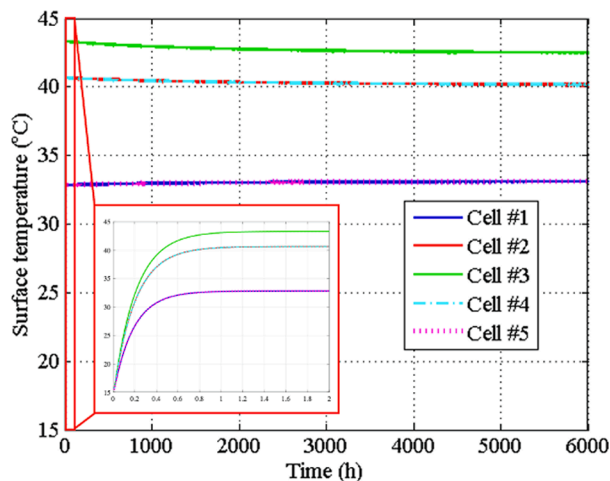
For the round cooling structure, both the temperature and capacity distributions of individual cells are symmetric while non-uniform, as

shown in Fig. 4. Cell #3, which is located in the middle of the coolant path, has the highest temperature and degradation due to its cooling condition. In contrast, the cells at the inlets of two coolant paths (i.e., Cell #1 and Cell #5) have the lowest temperature and degradation. The capacity variation under the round cooling structure is significantly reduced in comparison to the sequential cooling structure, as shown in Fig. 3 (d) and 4 (d). The cell with the lowest capacity (i.e., Cell #3) degrades more slowly than the one under the sequential cooling structure (Cell #5), indicating that the lifetime of battery strings can be extended by the round cooling structure. Specifically, assuming that the battery pack should be replaced when there is one cell reaching 80% of the initial capacity, the round cooling structure can extend the lifetime of battery string by 7% when compared to the sequential cooling structure, even though they have the same cooling capability (see Fig. 3 (c) and 4(c)). As mentioned above, the self-balancing mechanism will stabilize the cell-to-cell variation in terms of temperature and capacity under both the sequential and round cooling structures. For example, assuming that there is no initial variation among cells, the cell will diverge from each other due to uneven cooling structures. The cell with high temperature will have low resistance and high current, thereby
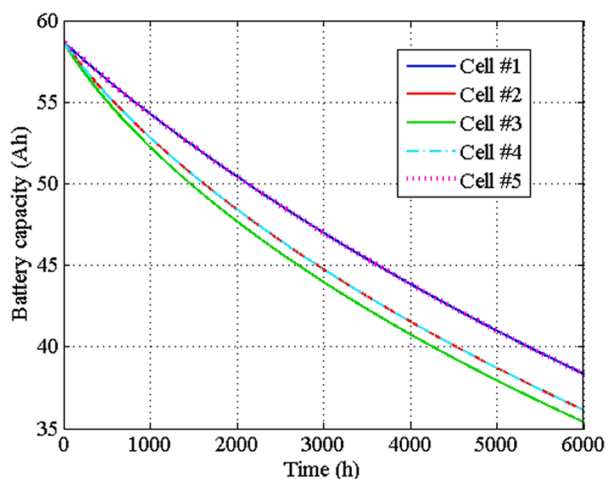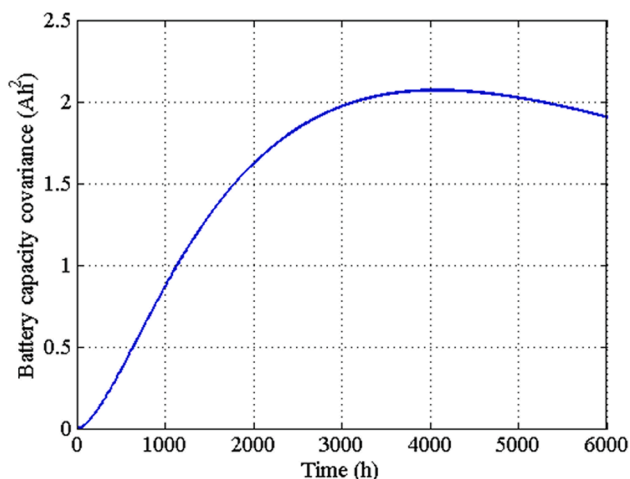
(a) Surface temperature

(b) Core temperature

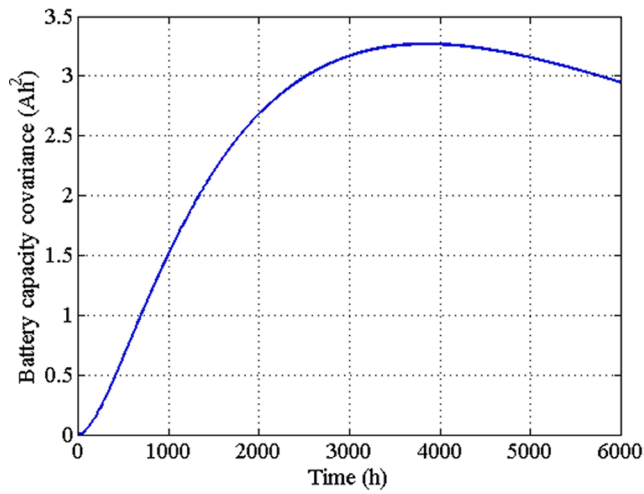(c) Cell capacities

(d) Capacity variation

Fig. 4. Temperature and Capacity Evolution of battery string (5 cells) under the round cooling structure.

aging faster than other cells. In consequence, the cell-to-cell variation will first increase over time, then due to the larger resistance, the aged cell will have higher resistance and therefore a low current, which will, in turn, reduce the degradation rate of the aged cell. In contrast, the degradation rate of the healthy cell will increase over time and generate more degradation than the aged cell. This interplay between electrical, thermal, and aging characteristics among cells provides a self-balancing effect (without control effort) and naturally suppresses the cell-to-cell variation, as shown in Figs. 3 and 4.
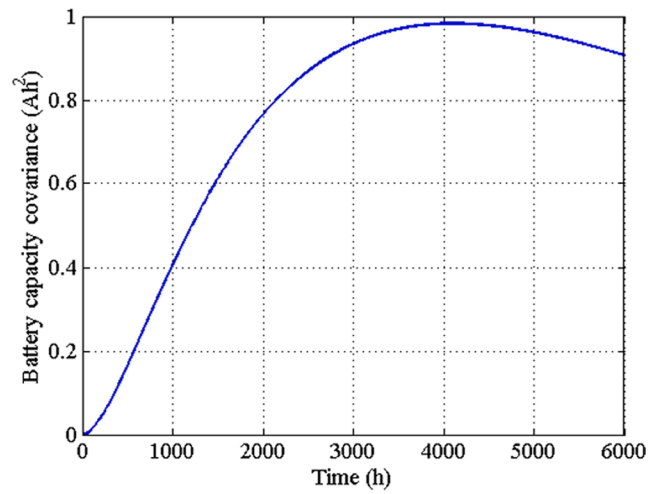
To further validate the conclusions obtained above, a larger battery string, including 20 cells, is also studied, and the results are shown in Fig. 5. Note that the heat capacity of coolant is increased proportionally, which can be realized by increasing the flow rate of coolant (i.e., V_{cool}). By comparing Fig. 3 (d) and Fig. 5 (a), the capacity variation under sequential cooling structure is almost the same in the two cases. For the round cooling structure, as shown in Fig. 4 (d) and Fig. 5 (b), the capacity variation is reduced when both the cell number and the flow rate of the coolant increase. This reveals that the round cooling structure is particularly favorable for reducing cell variation in large battery strings. All above simulations are conducted on a computer with a Core i7 processor (i.e., 2.6 GHz) and 32 GB RAM. With a fixed sampling time of

30 s, simulating the battery string with 5 cells over the 6000 h use case (see Fig. 3) roughly takes 4.5 h, while for the battery string with 20 cells, simulating the same use case (see Fig. 4) roughly takes 17 h. Hence, it is time-consuming to examine the progression of cell-to-cell variation, especially for a large battery string, due to the complex coupling relationship between the electrical, thermal, and aging models.

Even though the proposed electro-thermal-aging model provided in this paper is not verified by experimental results, similar trends of temperature distribution, i.e., divergence first and convergence later, can be found in the experimental study [50]. In addition, even though it is qualitatively obvious that the round cooling structure can better suppress the cell-to-cell variation due to its uniform cooling effect, a quantitative study of how the cell-to-cell variation progresses under different cooling structures can provide important information to select cooling structure in real applications, as vehicle companies need to balance performance and cost of the cooling system. In addition, this study can provide a quantitative basis to some following studies on how the cell-to-cell variation impacts battery pack-level performance and how much it should be regulated. In the battery industry, quantifying the cell-to-cell variation and its impact on system performance is important, no matter how the variation generates (e.g., manufacturing
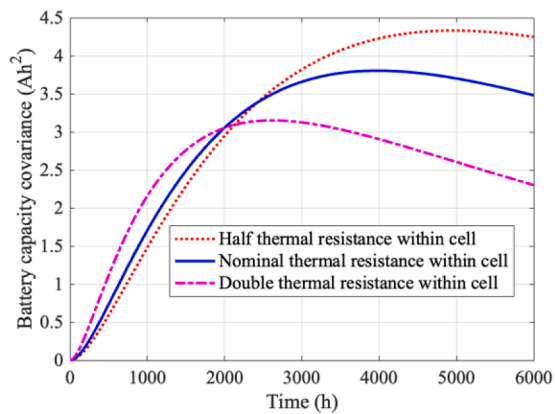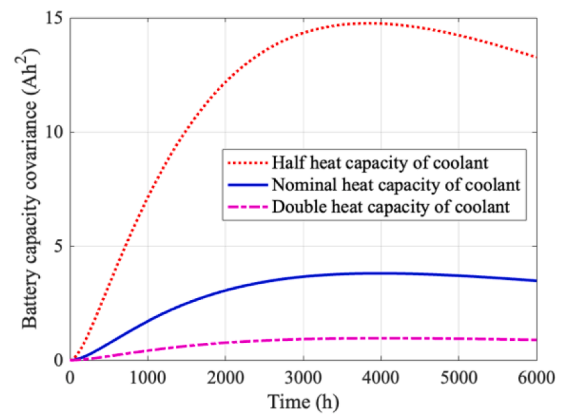
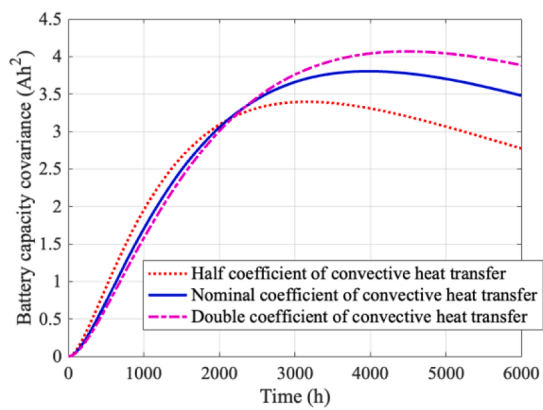(a) Sequential cooling structure

(b) Round cooling structure

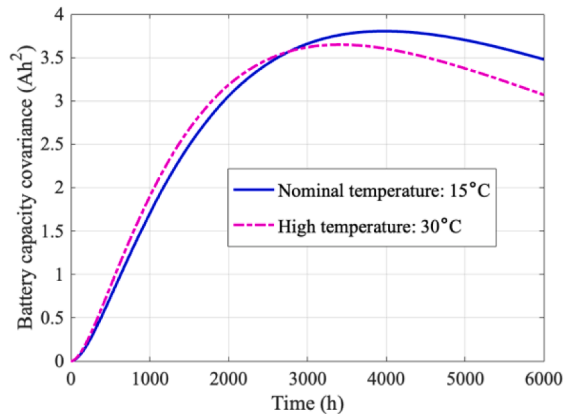**Fig. 5.** Capacity variation of battery string including 20 cells.

(a) Lumped thermal resistance within cell R_{in}

(b) Heat capacity of the flowing coolant C_f

(c) Coefficient of convective heat transfer between

coolant channel and cell surface h

(d) Environmental temperature

Fig. 6. Sensitivity analysis based on the battery string with 5 cells and sequential cooling structure.

inconsistency or uneven cooling condition during operation).

To examine the sensitivity of the above analysis results on the variations of cell parameters and operation conditions, we focus on the battery string, including 5 cells, under the sequential cooling structure

and change one variable each time to investigate its influence on the cell-to-cell variation. Specifically, four variables, including the lumped thermal resistance within cell R_{in}, heat capacity of the flowing coolant C_f, coefficient of convective heat transfer between coolant channel and
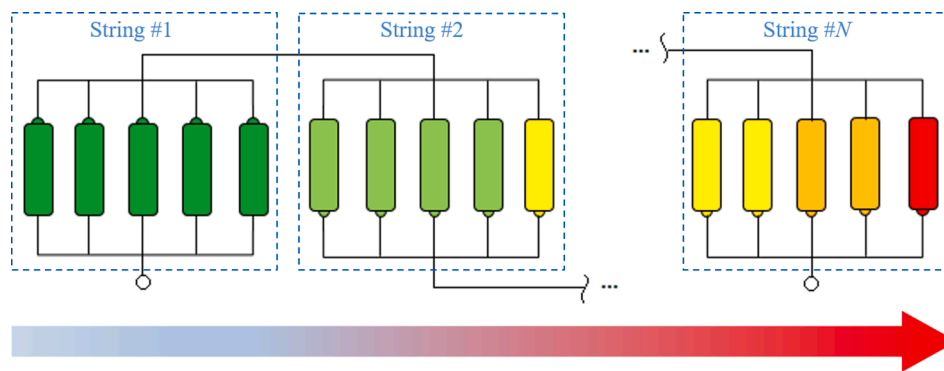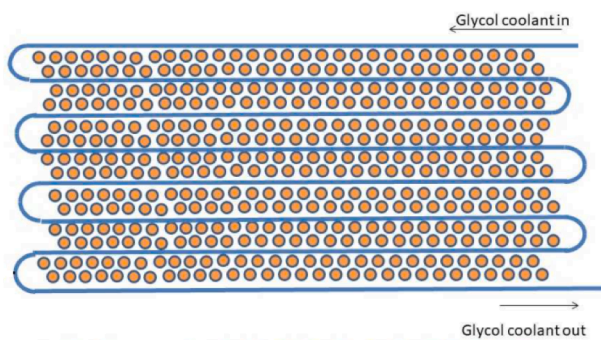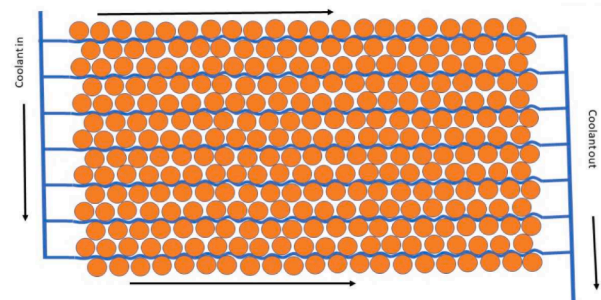
Fig. 7. Battery module with hybrid connections under sequential cooling structure.

(a) Tesla Model S (G. Bower [51])

(b) Tesla Model 3 (G. Bower [51])

(c) General Motors Chevy VOLT (GM [46])

Fig. 8. Practical cooling structures in electric vehicles.

cell surface h, and environmental temperature, are analyzed. When the lumped thermal resistance increases, it is more challenging to dissipate the heat from cell core to surface, and therefore the degradation as well as the cell-to-cell variation increase due to the high temperature, as shown in Fig. 6(a). However, large lumped thermal resistance will also reduce the heat exchange between cell surface and coolant channel. This will accordingly reduce the temperature gradient along coolant channel,

thereby reducing the cell-to-cell variation over time, as shown in Fig. 6 (a). Note that even though the cells are more consistent in the long term with a large lumped thermal resistance, the accumulative degradation of all cells increases due to the high inner temperature. As shown in Fig. 6 (b), the cell-to-cell variation can be significantly suppressed by improving the cooling capability, and a direct pathway is to increase the coolant flow rate. As shown in Fig. 6(c), the c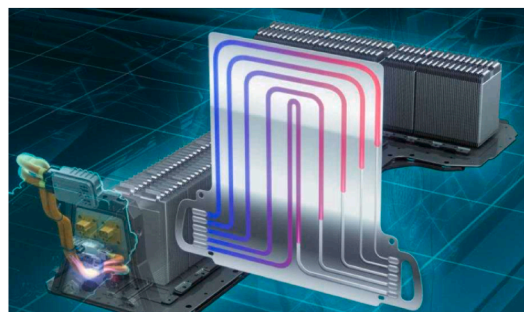oefficient of convective heat transfer between coolant channel and cell surface can impact the cell-to-cell variation in a similar way as the lumped thermal resistance (see Fig. 6(a)). A decreasing convective heat transfer will increase the cell degradation and cell-to-cell variation initially due to the high temperature at cell core, while it can reduce the cell-to-cell variation in the long term due to the less temperature gradient of coolant along its channel, meaning a more even cooling condition. Similarly, the higher environmental temperature will also increase the cell degradation and cell-to-cell variation first but improve the cell consistency in long term, as shown in Fig. 4(d). It shows that when environmental temperature increases, all cells in the battery string will age faster, but the cell consistency in the long term is not impaired, meaning that we will have a more aged but consistent battery string.

4. Discussion

In addition to parallel-connected cells, series-connected cells will also be addressed in this section, and some insights on real-world cooling structures in electric vehicles will be provided.

4.1. Series-connected cells

For parallel-connected cells, uneven current and temperature distributions contribute to the progression of capacity variation. Due to the existence of a self-balancing mechanism the capacity variation decreases after reaching the maximum value. For series-connected cells, only temperature imbalance exists, and there is no current imbalance as all cells have the same current. Therefore, cells with poor cooling conditions will have higher temperatures and larger degradation (i.e., lower capacity). In addition, those cells will subsequently have even higher temperatures as the heat generation is increased due to the increase in resistance. Even though the degradation curve is convex, self-balancing may not exist among series-connected cells, and the capacity variation will continuously increase, which is the main difference from parallel-connected cells. For practical battery modules which include both series and parallel connections (i.e., parallel first and then series connections), as shown in Fig. 7, the cell-to-cell variation within the battery strings (i.e., parallel-connected cells) will increase first and then decrease. Without a proper BMS, the string-to-string variation will continuously increase. In this case, the even cooling structure (e.g., round cooling structure) is highly preferred to suppress the capacity variation and improve the comprehensive performance of battery modules. In addition, the BMS should be carefully designed to monitor

the temperatures of individual cells and reduce the current of severely degraded cells with lower capacity and higher resistance.

4.2. Insights on practical cooling structures

The two cooling structures analyzed in this paper may slightly differ from practical cooling systems, e.g., in commercial EVs, which are designed considering many constraints such as capital cost and space limitations. As shown in Fig. 8, the cooling structures used in Tesla Model S, Model 3, and GM Chevy VOLT can be regarded as a sequential cooling structure, parallel-connected sequential cooling structure, and near-uniform cooling structure [46,51], respectively. The cooling system used in the Tesla Model S is the simplest, as shown in Fig. 8 (a). However, the temperature imbalance will be significant under aggressive current profiles (e.g., frequent acceleration/deceleration and high speed) as only one coolant path is deployed to cool 444 cylindrical cells. In the Tesla Model 3, the coolant path is split into several channels connected in parallel, and cells are more evenly cooled, as shown in Fig. 8 (b). Therefore, the temperature imbalance will be reduced, but the system cost may slightly increase.

The cooling system used in Chevy VOLT can provide the most uniform cooling conditions to all individual cells, as one aluminum cooling plate, which includes five coolant paths, is inserted between every two adjacent cells. All cells are cooled under similar condition, so the temperature imbalance will be well suppressed. For battery modules with a moderate number of large cells (i.e., high capacity), such near-uniform cooling system shown in Fig. 8 (c) is highly recommended, while for the battery pack of Tesla including a large number of smaller cells, this cooling system will significantly increase the cost and may be infeasible.

The round cooling structure (see Fig. 2(b)) studied in this paper has good performance in terms of providing even cooling conditions and suppressing cell-to-cell variation. Regarding the feasibility in practical applications, the round cooling structure can be approximated by slightly changing the current structures, such as the one shown in Fig. 8 (a). Two channels can be stacked together to create the double-direction coolant flows, and the heat transfer happening between channel/channel and channel/cell surface can both ensure a more uniform cooling condition. As a result, the cell-to-cell variation can be reduced with a minor cost increase caused by adding one more coolant channel. Moreover, on top of optimizing the cooling structure, the influence of cell-to-cell variation on battery pack performance should be further evaluated, and the benefit of reducing cell-to-cell variation should be quantified, as slight variation among cells may not influence the system-level efficiency and safety. To this end, for different applications, we should only control the cell-to-cell variation below a desired threshold rather than to 0, in order to balance the simplicity and effectiveness of the entire cooling system.

5. Conclusion

The cell-to-cell variation within parallel-connected cells under different cooling structures is analyzed in this paper. Simulation results show that under the sequential and round cooling structures, cell-to-cell variation increases first because of the non-uniform cooling conditions and then decreases and settles over time, thanks to the self-balancing effect within parallel-connected cells. The round cooling structure can significantly reduce the cell-to-cell variation compared to the sequential cooling structure, especially for long battery strings. These findings validate that the uniform cooling structure is preferred for reducing cell-to-cell variation; however, there may be some limitations in practical applications to achieve uniform cooling conditions. The trade-off between system cost and cell-to-cell variation needs to be carefully considered. Finally, series-connected battery cells are addressed, and several real-world cooling system structures are discussed and compared. In the future, we will establish the test bench, including the battery strings, different cooling systems, and high-power charging/

discharging tester, and experimentally validate the conclusions given in this paper.

CRediT authorship contribution statement

Ziyou Song: . **Niankai Yang:** . **Xinfan Lin:** . **Fanny Pinto Delgado:** . **Heath Hofmann:** Supervision. **Jing Sun:** Supervision.

Declaration of Competing Interest

The authors declare that they have no known competing financial interests or personal relationships that could have appeared to influence the work reported in this paper.

Acknowledgement

References

[1] Song Z, Feng S, Zhang L, Hu Z, Hu X, Yao R. Economy analysis of second-life battery in wind power systems considering battery degradation in dynamic processes: Real case scenarios. Appl Energy 2019;251:113411. https://doi.org/10.1016/j.apenergy.2019.113411.

[2] Shi W, Hu X, Jin C, Jiang J, Zhang Y, Yip T. Effects of imbalanced currents on large-format LiFePO4/graphite batteries systems connected in parallel. J Power Sources 2016;313:198–204.

[3] Zilberman I, Ludwig S, Jossen A. Cell-to-cell variation of calendar aging and reversible self-discharge in 18650 nickel-rich, silicon–graphite lithium-ion cells. J Storage Mater 2019;26:100900. https://doi.org/10.1016/j.est.2019.100900.

[4] Schuster SF, Brand MJ, Berg P, Gleissenberger M, Jossen A. Lithium-ion cell-to-cell variation during battery electric vehicle operation. J Power Sources 2015;297:242–51.

[5] Song Z, Hofmann H, Li J, Hou J, Han X, Ouyang M. Energy management strategies comparison for electric vehicles with hybrid energy storage system. Appl Energy 2014;134:321–31.

[6] Song, Z., Yang, X. G., Yang, N., Delgado, F. P., Hofmann, H., & Sun, J. (2020). A Study of Cell-to-Cell Variation of Capacity in Parallel-Connected Lithium-Ion Battery Cells. *eTransportation*, 100091.

[7] Kong X, Zheng Y, Ouyang M, Lu L, Li J, Zhang Z. Fault diagnosis and quantitative analysis of micro-short circuits for lithium-ion batteries in battery packs. J Power Sources 2018;395:358–68.

[8] Song, Z., Delgado, F. P., Hou, J., Hofmann, H., & Sun, J. (2020). Individual Cell Fault Detection for Parallel-Connected Battery Cells Based on the Statistical Model and Analysis. *arXiv preprint arXiv:2004.12412*.

[9] Lin X, Fu H, Perez HE, Siege JB, Stefanopoulou AG, Ding Yi, et al. Parameterization and observability analysis of scalable battery clusters for onboard thermal management. Oil & Gas Science and Technology-Revue d'IFP Energies nouvelles 2013;68(1):165–78.

[10] Saez-de-Ibarra A, Martinez-Laserna E, Stroe D-I, Swierczynski M, Rodriguez P. Sizing study of second life Li-ion batteries for enhancing renewable energy grid integration. IEEE Trans Ind Appl 2016;52(6):4999–5008.

[11] Paul S, Diegelmann C, Kabza H, Tillmetz W. Analysis of ageing inhomogeneities in lithium-ion battery systems. J Power Sources 2013;239:642–50.

[12] Chiu K-C, Lin C-H, Yeh S-F, Lin Y-H, Huang C-S, Chen K-C. Cycle life analysis of series connected lithium-ion batteries with temperature difference. J Power Sources 2014;263:75–84.

[13] Dubarry M, Pastor-Fernández C, Baure G, Yu TF, Widanage WD, Marco J. Battery energy storage system modeling: Investigation of intrinsic cell-to-cell variations. J Storage Mater 2019;23:19–28.

[14] Offer GJ, Yufit V, Howey DA, Wu B, Brandon NP. Module design and fault diagnosis in electric vehicle batteries. J Power Sources 2012;206:383–92.

[15] Feng X, Xu C, He X, Wang Li, Zhang G, Ouyang M. Mechanisms for the evolution of cell variations within a LiNixCoyMnzO2/graphite lithium-ion battery pack caused by temperature non-uniformity. J Cleaner Prod 2018;205:447–62.

[16] Bruen T, Marco J. Modelling and experimental evaluation of parallel connected lithium ion cells for an electric vehicle battery system. J Power Sources 2016;310:91–101.

[17] Yang N, Zhang X, Shang BinBin, Li G. Unbalanced discharging and aging due to temperature differences among the cells in a lithium-ion battery pack with parallel combination. J Power Sources 2016;306:733–41.

[18] Liu X, Ai W, Naylor Marlow M, Patel Y, Wu B. The effect of cell-to-cell variations and thermal gradients on the performance and degradation of lithium-ion battery packs. Appl Energy 2019;248:489–99.

[19] Feng F, Hu X, Hu L, Hu F, Li Y, Zhang L. Propagation mechanisms and diagnosis of parameter inconsistency within Li-Ion battery packs. Renew Sustain Energy Rev 2019;112:102–13.

[20] Tian J, Wang Y, Liu C, Chen Z. Consistency evaluation and cluster analysis for lithium-ion battery pack in electric vehicles. Energy 2020;194:116944. https://doi.org/10.1016/j.energy.2020.116944.

[21] Chang L, Zhang C, Wang T, Yu Z, Cui N, Duan B, et al. Correlations of cell-to-cell parameter variations on current and state-of-charge distributions within parallel-connected lithium-ion cells. J Power Sources 2019;437:226869. https://doi.org/10.1016/j.jpowsour.2019.226869.

[22] Baumann M, Wildfeuer L, Rohr S, Lienkamp M. Parameter variations within Li-Ion battery packs–Theoretical investigations and experimental quantification. J Storage Mater 2018;18:295–307.

[23] Rumpf K, Rheinfeld A, Schindler M, Keil J, Schua T, Jossen A. Influence of cell-to-cell variations on the inhomogeneity of lithium-ion battery modules. J Electrochem Soc 2018;165(11):A2587–607.

[24] Pastor-Fernández C, Bruen T, Widanage WD, Gama-Valdez MA, Marco J. A study of cell-to-cell interactions and degradation in parallel strings: implications for the battery management system. J Power Sources 2016;329:574–85.

[25] Gong X, Xiong R, Mi CC. Study of the characteristics of battery packs in electric vehicles with parallel-connected lithium-ion battery cells. IEEE Trans Ind Appl 2015;51(2):1872–9.

[26] Fill A, Koch S, Birke KP. Analytical model of the current distribution of parallel-connected battery cells and strings. J Storage Mater 2019;23:37–43.

[27] Fill A, Koch S, Birke KP. Algorithm for the detection of a single cell contact loss within parallel-connected cells based on continuous resistance ratio estimation. J Storage Mater 2020;27:101049. https://doi.org/10.1016/j.est.2019.101049.

[28] Cai Y, Cancian M, D'Arpino M, Rizzoni G. A generalized equivalent circuit model for large-scale battery packs with cell-to-cell variation. IEEE; 2019. p. 24–30.

[29] Han W, Altaf F, Zou C, Wik T. State of Power Prediction for Battery Systems with Parallel-Connected Units. IEEE Trans Transportation Electrification 2021.

[30] Hosseinzadeh E, Arias S, Krishna M, Worwood D, Barai A, Widanalage D, et al. Quantifying cell-to-cell variations of a parallel battery module for different pack configurations. Appl Energy 2021;282:115859. https://doi.org/10.1016/j.apenergy.2020.115859.

[31] Yang S, Gao X, Li Y, Xie W, Guo B, Zhang L, et al. Minimum lithium plating overpotential control based charging strategy for parallel battery module prevents side reactions. J Power Sources 2021;494:229772. https://doi.org/10.1016/j.jpowsour.2021.229772.

[32] Hu X, Li S, Peng H. A comparative study of equivalent circuit models for Li-ion batteries. J Power Sources 2012;198:359–67.

[33] Zhang Xi, Lu J, Yuan S, Yang J, Zhou X. A novel method for identification of lithium-ion battery equivalent circuit model parameters considering electrochemical properties. J Power Sources 2017;345:21–9.

[34] Song Z, Hou J, Li X, Wu X, Hu X, Hofmann H, et al. The sequential algorithm for combined state of charge and state of health estimation of lithium-ion battery based on active current injection. Energy 2020;193:116732. https://doi.org/10.1016/j.energy.2019.116732.

[35] Wei J, Dong G, Chen Z. Remaining useful life prediction and state of health diagnosis for lithium-ion batteries using particle filter and support vector regression. IEEE Trans Ind Electron 2018;65(7):5634–43.

[36] Lin X, Perez HE, Mohan S, Siegel JB, Stefanopoulou AG, Ding Yi, et al. A lumped-parameter electro-thermal model for cylindrical batteries. J Power Sources 2014;257:1–11.

[37] Lin X, Perez HE, Siegel JB, Stefanopoulou AG, Li Y, Anderson RD, et al. Online parameterization of lumped thermal dynamics in cylindrical lithium ion batteries for core temperature estimation and health monitoring. IEEE Trans Control Syst Technol 2012;21(5):1745–55.

[38] Smith K, Wang C-Y. Power and thermal characterization of a lithium-ion battery pack for hybrid-electric vehicles. J Power Sources 2006;160(1):662–73.

[39] Gu WB, Wang CY. Thermal-electrochemical modeling of battery systems. J Electrochem Soc 2000;147(8):2910. https://doi.org/10.1149/1.1393625.

[40] Farag M, Sweity H, Fleckenstein M, Habibi S. Combined electrochemical, heat generation, and thermal model for large prismatic lithium-ion batteries in real-time applications. J Power Sources 2017;360:618–33.

[41] Yang X-G, Leng Y, Zhang G, Ge S, Wang C-Y. Modeling of lithium plating induced aging of lithium-ion batteries: Transition from linear to nonlinear aging. J Power Sources 2017;360:28–40.

[42] Schuster SF, Bach T, Fleder E, Müller J, Brand M, Sextl G, et al. Nonlinear aging characteristics of lithium-ion cells under different operational conditions. J Storage Mater 2015;1:44–53.

[43] Wang J, Liu P, Hicks-Garner J, Sherman E, Soukiazian S, Verbrugge M, et al. Cycle-life model for graphite-LiFePO4 cells. J Power Sources 2011;196(8):3942–8.

[44] Song Z, Li J, Han X, Xu L, Lu L, Ouyang M, et al. Multi-objective optimization of a semi-active battery/supercapacitor energy storage system for electric vehicles. Appl Energy 2014;135:212–24.

[45] Safari M, Morcrette M, Teyssot A, Delacourt C. Life-prediction methods for lithium-ion batteries derived from a fatigue approach: I. introduction: capacity-loss prediction based on damage accumulation. J Electrochem Soc 2010;157(6):A713.

[46] Bower, G. (2015). Tesla or GM: Who has the best battery thermal management?. *Inside EVs*; Available from: http://insideevs.com/tesla-or-gm-who-has-the-best-battery-thermal-management-bower/.

[47] Lin X, Perez HE, Siegel JB, Stefanopoulou AG. Robust estimation of battery system temperature distribution under sparse sensing and uncertainty. IEEE Trans Control Syst Technol 2020;28(3):753–65.

[48] Darcovich K, MacNeil DD, Recoskie S, Kenney B. Coupled electrochemical and thermal battery models for thermal management of prismatic automotive cells. Appl Therm Eng 2018;133:566–75.

[49] Han X, Ouyang M, Lu L, Li J. A comparative study of commercial lithium ion battery cycle life in electric vehicle: Capacity loss estimation. J Power Sources 2014;268:658–69.

[50] Luca R, Whiteley M, Neville T, Tranter T, Weaving J, Marco J, et al. Current Imbalance in Parallel Battery Strings Measured Using a Hall-Effect Sensor Array. Energy Technology 2021;9(4):2001014. https://doi.org/10.1002/ente.v9.410.1002/ente.202001014.

[51] Bower, G. (2018). Tesla Model 3 Battery Cooling Much-Improved ... Track Mode?. *Inside EVs*; Available from: https://insideevs.com/news/338711/tesla-model-3-battery-cooling-much-improved-track-mode/.